

RESEARCH ARTICLE

High-field ex vivo and in vivo two-dimensional nuclear magnetic resonance spectroscopy in murine brain: Resolving and exploring the molecular environment

Ricardo P. Martinho | Mukul G. Jain | Lucio Frydman 

Department of Chemical and Biological Physics, Weizmann Institute of Science, Rehovot, Israel

Correspondence

Lucio Frydman, Department of Chemical and Biological Physics, Weizmann Institute of Science, Rehovot, Israel.

Email: lucio.frydman@weizmann.ac.il

Funding information

Clore Institute for Magnetic Resonance (Weizmann Institute). Israel Science Foundation; Grant Numbers: 3594/21 and 1874/22. EU Horizon 2020 Programme; Marie Skłodowska-Curie Grant 642773 and FET-OPEN PATHOS grant 828946

The structural and chemical complexities within the brain pose a challenge that few noninvasive techniques can tackle with the dexterity of nuclear magnetic resonance (NMR) spectroscopy. Still, even with the advent of ultrahigh fields and of cryogenically cooled coils for in vivo research, the superposition of metabolic resonances arising from the brain remains a challenge. The present study explores the potential to tackle this milieu using a combination of two-dimensional (2D) NMR techniques, implemented on murine brains in vivo at 15.2 T and ex vivo at 14.1 T. While both experiments were affected by substantial inhomogeneous broadenings conveying distinct elongated lineshapes to the cross-peaks, the ability of increased fields to resolve off-diagonal resonances was clear. A comparison between the corresponding conventional and double quantum-filtered correlated spectroscopy traces enabled an improved assignment of in vivo resonances on the basis of more sensitive ex vivo 2D acquisitions, foremost on the basis of homonuclear cross-relaxation-driven correlations for peaks resonating downfield from water, and of heteronuclear correlations at natural abundance for the upfield protons. With the aid of such 2D correlations approximately 29 metabolites could be resolved and identified. This enhanced resolution was used to explore features related to the metabolites' diffusivities, their exposure to water, and their facility to undergo magnetization transfers to amide/amine/hydroxyl resonances. Cross-peaks from main murine brain biomolecules, including choline, creatine, γ -aminobutyric acid, N-acetyl aspartate, glutamine, and glutamate, showed enhancements in several of these various features, opening interesting vistas about metabolite compartmentalization as viewed by these 2D NMR experiments.

KEYWORDS

brain metabolites, chemical exchange, COSY, diffusivity, HSQC, magnetization transfer, multidimensional NMR

Abbreviations: Ace, acetate; Ala, alanine; Arg, arginine; Asp, aspartate; CEST, chemical exchange saturation transfer; Cho, choline; COSY, correlation spectroscopy; Cre, creatine; CT, constant time; Cys, cysteine; DQF, double quantum filtered; DW, diffusion weighted; ETA, ethanolamine; GABA, γ -aminobutyric acid; GL, glycerol; Glc, glucose; Gln, glutamine; Glu, glutamate; Gly, glycine; GSH, glutathione; HSQC, heteronuclear single quantum correlation spectroscopy; L-PROSY, looped projected spectroscopy; Lac, lactate; Leu, leucine; Lys, lysine; Met, methionine; MRI, magnetic resonance imaging; MT, magnetization transfer; Myo, myo-inositol; NAA, N-acetyl aspartate; NMR, nuclear magnetic resonance; NOESY, nuclear overhauser effect spectroscopy; PCh, phosphorylcholine; PE, phosphoethanolamine; Pro, proline; Ser, serine; Suc, succinate; SW, spectral width; Tau, taurine; Thr, threonine; TOCSY, total correlation spectroscopy; Val, valine; WEX, Water Exchange; WG, WATERGATE; 2D, two dimensional.

This is an open access article under the terms of the [Creative Commons Attribution-NonCommercial-NoDerivs](https://creativecommons.org/licenses/by-nc-nd/4.0/) License, which permits use and distribution in any medium, provided the original work is properly cited, the use is non-commercial and no modifications or adaptations are made.

© 2022 The Authors. *NMR in Biomedicine* published by John Wiley & Sons Ltd.

1 | INTRODUCTION

Nuclear magnetic resonance (NMR) opens a number of routes for minimally invasive, *in vivo* brain investigations. In its imaging mode (MRI), NMR delivers high resolution anatomies from animals and humans, based on the observation of the abundant water ^1H signal. Contrast mechanisms such as relaxation or diffusion can then discern local morphologies, distinguish normal from diseased tissues, and elucidate brain connectivity.^{1,2} Brain activities, however, are driven by metabolic changes, associated with changes in the neurochemical profile. These are best studied by the second main route opened by *in vivo* NMR, spectroscopy,^{3–7} which can be carried out in either a localized or a spectroscopic imaging mode. Resolved ^1H signals can then characterize neurotransmitters such as N-acetyl aspartate (NAA) or glutamate, molecules involved in energetics such as creatine (Cre), and macromolecules including proteins and lipids. Once metabolic resonances are resolved and assigned, NMR spectra can provide insights that are unavailable with water-based observations: concentrations deriving from peak intensities, viscosity and binding characteristics via relaxation times, and microstructural information by assessments of diffusivity.^{3–10} Relaxation properties can also be probed by phenomena such as magnetization transfer (MT), including cross-relaxation with an NMR-invisible pool made up of semisolid proteins and lipids,^{11–13} as well as chemical exchanges with the solvent (as in chemical exchange saturation transfer [CEST]),^{14–17} which enable the indirect observation of moieties in small and large molecules.^{18–21}

Despite this potential, resolving and characterizing brain metabolic resonances is hampered by the large number of compounds present, by signal overlap among multiplets, by susceptibility broadening, and by limited sensitivity. High magnetic fields have alleviated some of these limitations,^{22,23} enabling the detection and quantification of up to 21 metabolites *in vivo* for murine brains.^{4,24} Resolving these metabolic signatures usually requires spectral fitting to basis sets,²⁵ as well as various forms of spectral editing.^{26,27} Even further spectral resolution could arise from two-dimensional (2D) spectroscopy,^{28,29} spreading peaks over a larger frequency space. Because of their long duration and limited sensitivity, such experiments are usually carried out *in vivo* using spatial localization,^{27,30,31} with ^1H - ^1H correlated spectroscopy providing insights regarding metabolites such as NAA, glutamine and glutamate (Gln/Glu), glutathione (GSH), and choline (Cho). The current study extends such 2D observations with experiments performed *in vivo* at 15.2 T. Despite relying on cryogenic coils and high fields, these *in vivo* murine brain experiments were still sensitivity limited, primarily because of a low coil filling factor, and because of the limited duration over which acquisitions could be signal averaged. *In vivo* experiments were therefore complemented by 2D *ex vivo* excised brain observations carried out at 14.1 T, with credence for the usefulness of *ex vivo* measurements provided by similar 2D double quantum-filtered (DQF) and regular localized correlated spectroscopy (COSY) sets obtained on living and excised brains. To further probe the environments and properties of the metabolites thus resolved, high-resolution 2D NMR experiments—foremost heteronuclear ^1H - ^{13}C natural abundance correlations—were combined with MT, water-exchange, and diffusivity contrasts. These pseudo-3D NMR experiments provided insights concerning the interactions that metabolites, including Cho, Cre, NAA, Glu, myo-inositol (Myo), taurine (Tau), and γ -aminobutyric acid (GABA), experienced in the tissue.

2 | MATERIALS AND METHODS

2.1 | Animal preparation

Animal experiments were preapproved by the Weizmann Institute's IACUC, which is fully accredited by the AAALAC, the US NIH Office of Laboratory Animal Welfare and the Israel Ministry of Health. Healthy male C57BL/6 mice aged ~6 months were used in the study, both for the *in vivo* ($n = 4$) and *ex vivo* ($n = 4$) experiments (with different mice used for the *in vivo* and *ex vivo* experiments). For the *ex vivo* experiments, the animals were sacrificed by cervical dislocation; their brains were then removed, and carefully submerged in their entirety in Fluorinert FC-770 (3 M, Zwijndrecht, Belgium), a proton-free fluid that minimizes susceptibility artifacts and has little impact on a tissue's histochemical properties.^{32,33} Such immersed brains were placed—without fixation—inside 5-mm Shigemitsu tubes (Wilmad Labglass, Vineland, NJ, USA), for the purpose of improving the field homogeneity over our small specimens. Experiments were only performed within the first 8 h postremoval of the brains to avoid, in as much as possible, sample decomposition.

2.2 | Experimental details

2.2.1 | *Ex vivo* NMR

Ex vivo data were acquired on a 14.1-T Bruker spectrometer equipped with an Avance IIIHD console and a TCI Prodigy cold probe. All experiments were performed at 25°C without locking the ^2H channel (the magnet field drift was <0.5 Hz/h for ^1H and was disregarded). To facilitate comparisons with the *in vivo* data, ^1H spectra were referenced by the frequency of water at 25°C (4.82 ppm), which in turn was externally referenced by sodium trimethylsilylpropanesulfonate (DSS).³⁴ ^{13}C spectra were referenced by setting the methyl resonance of lactate to 22.903 ppm,^{35,36} which in turn was externally referenced by DSS.

Excised brains were initially assessed by one-dimensional (1D) ^1H NMR at 600 MHz using a WATERGATE-3919 (WG) water-suppressed sequence,^{37,38} employing a 1.5-ms flipback pulse at the start, a 90- μs delay for binomial water suppression, and an echo time around the 3919 composite pulse of 400 μs . To acquire T_2 -weighted spectra, a water suppression based on the perfect echo sequence with W5 (PEW5) and a 90- μs delay for binomial water suppression was employed,³⁹ for a total echo time of 40 ms. For MT acquisitions these sequences were preceded by a 2-s continuous wave (CW) saturation field B_1 of 1 μT , whose frequency was stepped by 0.1 ppm from 10.7 to -1.3 ppm; these WG-MT and PEW5-MT scans also used two averages.

Table 1 describes the ex vivo 2D NMR experiments performed, together with their main parameters. These included: (i) Looped projected spectroscopy (L-PROSY) 2D ^1H - ^1H nuclear Overhauser effect spectroscopy (NOESY)⁴⁰ using 4.12-ms Q5 90° selective pulses at 7.75 ppm for encoding,⁴¹ WG for solvent suppression, six looped mixing times of 100 ms for nuclear Overhauser effect (NOE) buildup, and four phase-cycled averages. (ii) ^1H - ^1H DQF-COSY,^{42,43} with a 4:3:10 gradient-based coherence selection scheme and four phase-cycled averages per t_1 point. (iii) ^1H - ^1H total correlation spectroscopy (TOCSY) with a 48-ms long, 5-kHz strong DIPSI-2 sequence for isotropic mixing,⁴⁴ WG solvent suppression with the aforementioned parameters, and four phase-cycled averages per t_1 point. (iv) Fully decoupled ^1H - ^{13}C Heteronuclear Single Quantum Coherence Spectroscopy (HSQC) experiments with double INEPT transfers tuned to $J = 140$ Hz, echo/antiecho gradient selection, and two phase-cycled scans per t_1 point. (v) ^1H - ^{13}C HSQC experiments incorporating a modified Water EXchange filter (WEX) that selects ^1H - ^{13}C pairs associated with water exchanges of neighboring ^1H s,⁴⁵ based on a pair of water-selective 90° sinc pulses (with one of them phase cycled along with the receiver as x, -x), an 800-ms mixing time to relay the WEX information, and eight averages per HSQC t_1 point. (vi) ^1H - ^{13}C HSQC experiments incorporating an MT module (MT-HSQC), performed using a 2-s CW $B_1 = 1$ μT saturating field placed at either 6.7 or 8.2 ppm, and four phase-cycled averages; the output of these scans was subtracted from identical experiments involving the same timings but no saturation, in order to observe the moieties affected by the CW irradiation. (vii) ^1H - ^{13}C HSQC experiments incorporating diffusion weighting via a constant time, stimulated-echo, bipolar gradient pulsed sequence,⁴⁶ using 2-ms diffusion gradient pulses of 5 and 25 G/cm, separated by a diffusion time of 21.7 ms; in order to account for the loss of sensitivity because of the diffusion weighting, each experiment was performed in eight blocks of four averages, which alternated between high and low b-valued experiments; these were then suitably combined, in order to highlight fast-diffusing ^1H - ^{13}C pairs.

Spectra were processed using Bruker Topspin or NMRFAM-SPARKY.⁴⁷

2.2.2 | In vivo NMR

In vivo experiments were performed on a horizontal Bruker Biospec 15.2-T USR preclinical MRI scanner with an Avance IIIHD console and a B-GA 6S-100 three-axis gradient system with a 60-mm inner diameter, supporting a maximum gradient strength of 1000 mT/m. Data were acquired

TABLE 1 2D experiments and main parameters run at 14.1 T on ex vivo samples. Index 1 corresponds to the indirect dimension, index 2 corresponds to the direct dimension; also indicated are the goals of the experiments and the figures presenting their data

Experiment	Description	SW1 (ppm)	t_1 points	SW2 (ppm)	t_2 points	Experimental time	Figure
^1H - ^1H L-PROSY	Correlation between exchanging and aliphatic protons	11	256	11	1024	1 h 5 min	4A
^1H - ^1H DQF-COSY	Correlation between J-coupled protons	12	256	12	4096	57 min	2B
^1H - ^1H TOCSY	Correlation between protons in the same spin system	12	256	12	4096	1 h 15 min	2C
^1H - ^{13}C HSQC	Correlation between bound protons and carbons	80	256	16	2048	54 min	2A
^1H - ^{13}C WEX-HSQC	Correlation between protons receiving polarization from water, and bound carbons	80	256	16	2048	2 h 15 min	6A
^1H - ^{13}C MT-HSQC	Correlation between protons affected by the saturation of a neighboring labile ^1H , and their bonded carbons	80	128	16	2048	1 h 30 min	6C
^1H - ^{13}C DW-HSQC	Correlation between bound protons and carbons of faster diffusing species	80	128	16	2048	7 h 31 min	6B

Abbreviations: COSY, correlated spectroscopy; DQF, double quantum-filtered; DW, diffusion-weighted; HSQC, Heteronuclear Single Quantum Coherence Spectroscopy; L-PROSY, looped projected spectroscopy; MT, magnetization transfer; SW1, indirect-domain spectral width; SW2, direct-domain spectral width; t_1 , indirect-domain time; t_2 , direct-domain time; TOCSY, total correlation spectroscopy; WEX, Water EXchange filter.

with a surface ^1H 650-MHz quadrature transmit/receive cryocoil with an inner diameter of 20 mm. Mice were immobilized employing a tooth bar and ear bars ensuring minimal motion; they were kept under isoflurane (1%–2%) anesthesia through a vaporizer, and maintained at a constant $\sim 36^\circ\text{C}$ temperature with a water bath while being monitored via a rectal thermometer. Respiration was monitored via a pressure sensor (SA-II, Stony Brook, NY, USA) and maintained at ~ 100 breaths/min. A $4 \times 3 \times 6 \text{ mm}^3$ ($72\text{-}\mu\text{l}$) voxel was localized in the center of the brain in order to encompass most of its mass while staying clear from edges, and experiments on these voxels were run after shimming their water linewidths to 30 Hz or less. All data had their frequencies referenced to the 4.71-ppm peak of a nonwater-suppressed PRESS spectrum, acquired on the animal at 36°C immediately before each experiment. All localized 2D COSYs were performed using Shinnar-LeRoux pulses (SLR, 10 kHz bandwidth) for localization, 256 t_1 points to encode the indirect domain, and spectral widths of 9.24 ppm. DQF-COSYs were recorded with 12.0-ppm spectral widths. All 2D acquisitions were performed in eight blocks, lasting ~ 18 min each and involving the sampling of all t_1 points, with two averages for each. These blocks were subsequently registered to one another according to the dominant resonance of water, and co-added (in Matlab) so as to minimize losses that would arise in longer signal averaging times from artifacts such as motion or field drifts. All chemical shifts were referenced to the water ^1H peak.

3 | RESULTS

3.1 | Validation of the ex vivo protocol

The sensitivity improvements arising from significantly higher coil filling factors and from the possibility of averaging over long acquisition times, makes ex vivo NMR studies of brain metabolites easier than under in vivo conditions. Relevance, however, requires performing NMR investigations in vivo. In order to bridge this gap between performance and pertinence, the outcomes of a number of experiments were compared under both conditions. Figure 1 shows some of these, with water-suppressed 1D and 2D ^1H NMR spectra collected for these two cases. The main difference between the two is naturally the very different sensitivities, reflecting foremost the larger volume of the ex vivo sample. This is easily appreciated in the downfield 5–10 ppm region, where limited sensitivity and the use of VAPOR water suppression leads in vivo to a nearly null signal. Although the two water-suppressed spectra present similarities in their upfield (0.5–4.6 ppm) regions, quantitative differences can also be observed. One of the main differences is, as expected, a heightened peak intensity at ~ 1.31 ppm, corresponding to lactate's postmortem increase⁴⁸; changes can also be observed in the intensities of the other main metabolites, as summarized in part in Table S1.

3.2 | Assignment of upfield brain ^1H resonances by ex vivo 2D NMR

Given the overall resemblance between the 1D and 2D ^1H NMR sets compared in Figure 1, we sought to combine the sensitivity advantages of high-field ex vivo acquisitions with the resolution brought about by 2D NMR, for exploring additional assignment and characterization possibilities. Figure 2 summarizes results from three such tests performed on an intact excised brain: one correlating adjacent protons via DQF-COSY, another reporting protons within a mutually coupled spin system by ^1H - ^1H TOCSY, and a third separating peaks according to the joint ^1H and ^{13}C shifts of directly bonded spin pairs via HSQC. These spectra are similar to those that can be expected from the same acquisitions on extracted metabolites,^{49,50} albeit with line widths that are intrinsically broadened by susceptibility effects—and with all the advantages and disadvantages of examining a milieu that has not been subject to a biased extraction.⁵¹ The susceptibility broadenings are particularly evident in the homonuclear correlations (Figure 2B,C), as they affect peak shapes to the same degree along both dimensions, endowing off-diagonal cross-peaks with elongated lineshapes running parallel to the main diagonal. Although harder to appreciate in Figure 2A, similar peak distortions arise in the heteronuclear correlation. Presented in Figure S1 is a sample consistency test, showing two 2D HSQC brain spectra acquired from different mice at different times postextraction; the good agreement among these lends credence to the reproducibility (and relevance) of these acquisitions.

The TOCSY correlation in Figure 2 has remarkably good sensitivity—equal to or better than its DQF-COSY counterpart—but yields too much overlap among the off-diagonal cross-peaks to be a practical alternative. The highest spectral resolution is clearly provided by HSQC, thanks to the spread arising along the ^{13}C dimension; this has also been recently noted in excised tissue experiments.⁵² For the 2D HSQC correlation in Figure 2A, upwards of 90 identifiable cross-peaks can be distinguished for the upfield ^1H region. An assignment of these peaks was performed based on chemical shift values described in the Human Metabolome Database^{35,36} and by Park et al.,⁵³ and was further validated by ^1H - ^1H cross-peaks. In total, 89 resonances could be assigned for the HSQC spectra, arising from either 28 or 29 molecules (the uncertainty resulting from the overlap between Cre and phosphocreatine). Cross-peak assignments for the various 2D ^1H - ^1H spectra were also derived from these datasets; they are indicated in Figure 2 for the ex vivo acquisitions, and in Figure 3 for an illustrative ^1H 1D localized brain spectrum acquired in vivo at 15.2 T. The ensuing chemical shifts are summarized in Table S2; they include metabolites such as lactate or acetate whose peaks are probably heightened by the ex vivo conditions of the runs,⁷ and metabolites like succinate that could be unambiguously assigned by their distinct shifts despite yielding single HSQC cross-peaks. Close to water, however, a number of resonances (most likely belonging to sugars) could not be

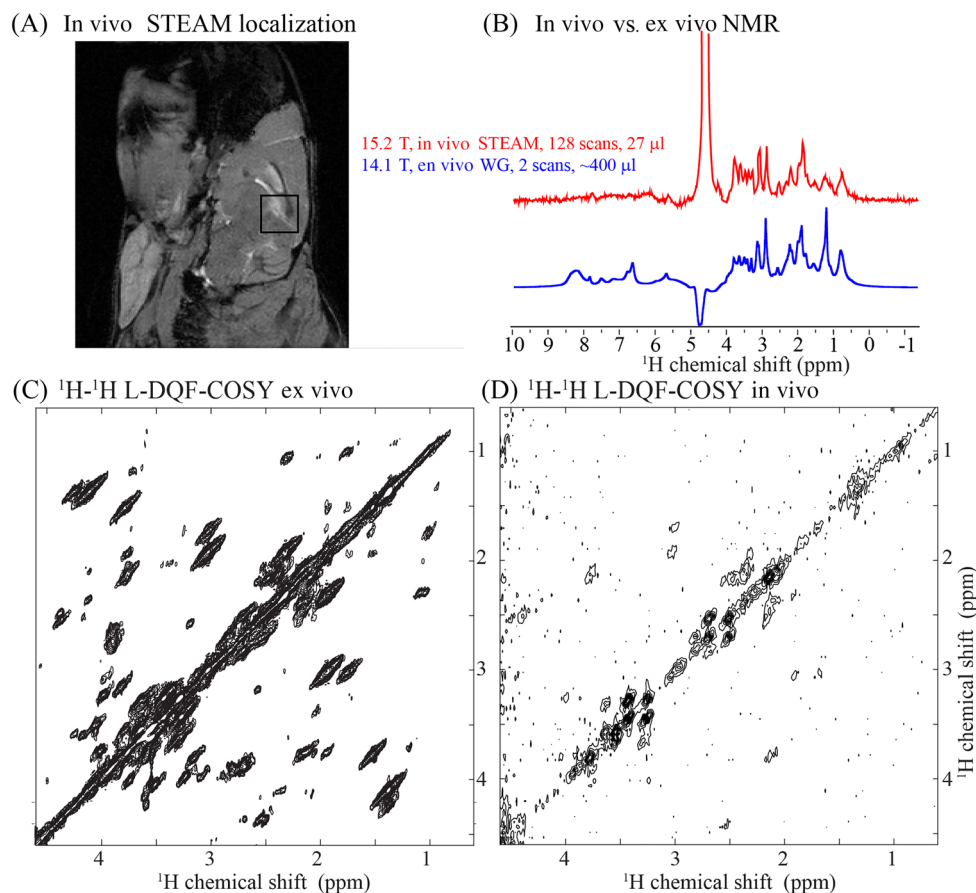


FIGURE 1 (A) FLASH image of a mouse brain acquired in vivo highlighting the voxel $3 \times 3 \times 3 \text{ mm}^3$ used for STEAM localization. (B) Comparison between a localized STEAM spectrum obtained in vivo at 15.2 T with VAPOR-based water suppression, and a spectrum obtained ex vivo using WG at 14.1 T (both with 2-s recycle delay). (C) and (D) Comparison between in vivo and ex vivo DQF-COSY results acquired in the mouse brain. (C) DQF-COSY acquired at 14.1 T in $\sim 400 \mu\text{l}$ volume (57 min); (D) L-DQF-COSY obtained in a 72- μl volume (2 h 24 min). The latter dataset is further analyzed in Figure 5. DQF-COSY, double quantum-filtered correlated spectroscopy; FLASH, Fast Low-Angle SHot; L-DQF-COSY, localized double quantum-filtered correlated spectroscopy; STEAM, STimulated Echo Acquisition Mode; VAPOR, VArIable Power radiofrequency pulses with Optimized Relaxation delays; WG, WATERGATE-3919

unambiguously identified, including a peak common to glucose and to other molecules (e.g., glycogen) highlighted as Glc*. Additional HSQC and COSY cross-peaks that could not be assigned likely belong to lipids or macromolecules, like the upfield ^1H resonances at $\sim 0.8 \text{ ppm}$.

Three downfield-upfield ^1H - ^1H cross-peaks are shown in the lower inset of Figure 2B. Two of these match shifts reported for NAA (7.98–4.13 ppm)⁷ and GSH (8.25–3.76 ppm)⁵⁴; the remainder was tentatively assigned to proline (7.98–4.13 ppm), as it matches the position expected for its amine resonance.⁵⁵ Protons originating these downfield peaks are likely to undergo fast exchanges with water, which compromises their study by J-based 2D correlations. Instead, the potential of high-field 2D correlations was explored using cross-relaxation-based experiments, reporting on the spatial proximity among different groups. As intramolecular cross-relaxation is also attenuated by exchanges with the solvent, these correlations relied on L-PROSY NOESY,⁴⁰ a time-domain encoding yielding 2D NOE correlations but delivering higher cross-peak intensities than conventional NOESY for fast solvent-exchanging protons (as exemplified in Figure S2). Correlations between downfield and upfield resonances were also investigated with MT experiments, where selected frequencies were presaturated, stepwise and in different scans, in a CW fashion; the effects of these saturations were then followed on the water-suppressed ^1H spectra of the different metabolites, when collected with long and short echo times (see Figure S3 for the echo times' differential effects).^{56–58}

The 2D L-PROSY NOESY spectra collected on excised murine brains (Figure 4A) resolved a series of cross-peaks centered at indirect-domain frequencies $F_1 = 6.6, 6.7, \text{ and } 7.7 \text{ ppm}$, which on the basis of literature data⁵⁵ were assigned to intramolecular NAA, Gln, and Cre correlations. Dominating the 2D L-PROSY NOESY, however, is a relatively broad feature correlated with a downfield resonance at $F_1 \approx 8.2 \text{ ppm}$, eliciting multiple correlations with peaks in the $F_2 = 1\text{--}4 \text{ ppm}$ region. Figure 4B compares the L-PROSY NOESY slice extracted at this $F_1 = 8.2 \text{ ppm}$ position, with MT results arising upon observing the same resonance in a series of frequency-incremented experiments. Apart from a water saturation dip visible in the 1D but not in the water-suppressed 2D NMR experiments, and of wider intrinsic lineshapes convoluting the MT measurements because of the CW irradiation, the similarity between the two cross sections is evident (Figure 4B). The cross-peak patterns arising in the 1–2 and

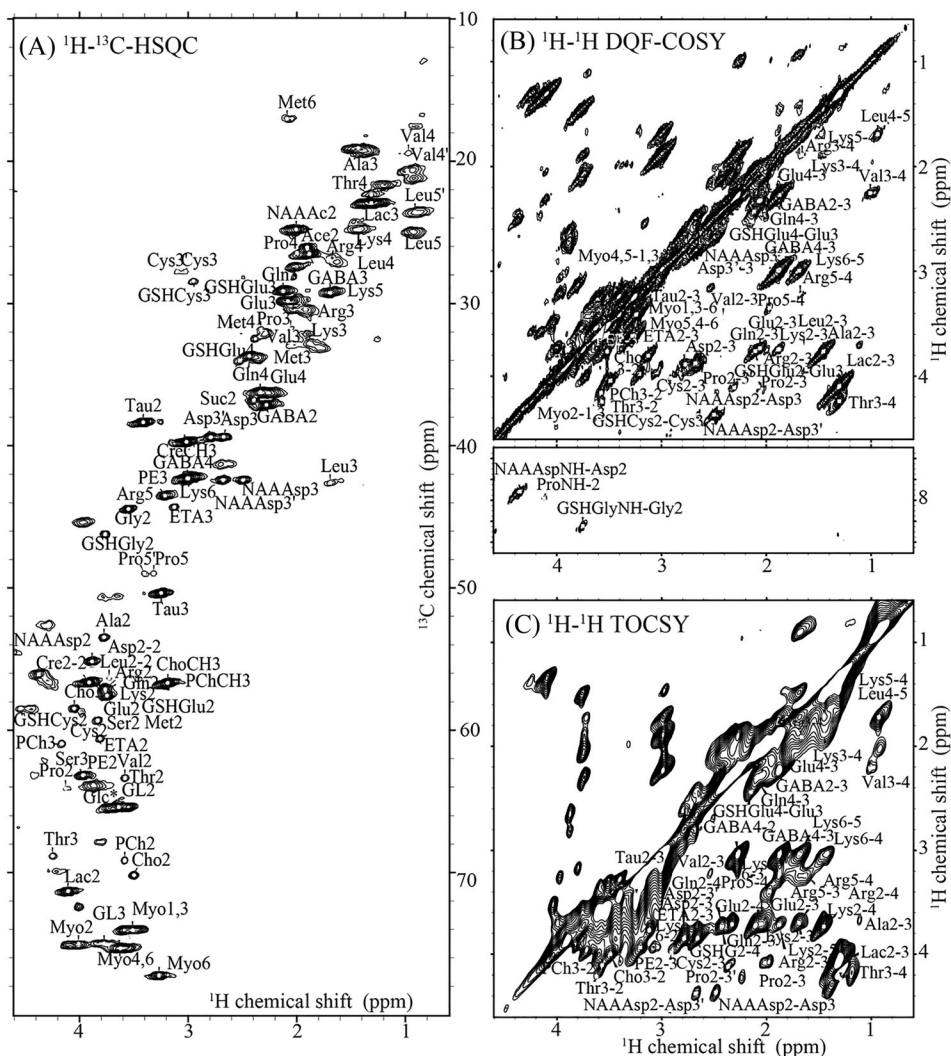


FIGURE 2 2D correlation experiments performed on an excised mouse brain at 14.1 T. (A) ^1H - ^{13}C HSQC (54 min); (B) DQF-COSY (57 min); and (C) TOCSY (1 h 14 min). Also shown are assignments of various cross-peaks. Ace, acetate; Ala, alanine; Arg, arginine; Asp, aspartate; Cho, choline; Cre, creatine (overlaps with phosphocreatine); Cys, cysteine; DQF-COSY, double quantum-filtered correlation spectroscopy; ETA, ethanalamine; GABA, γ -aminobutyric acid; GL, glycerol; Glc, glucose (peak may be common to other sugars); Gln, glutamine; Glu, glutamate; Gly, glycine; GSH, glutathione; HSQC, Heteronuclear Single Quantum Coherence Spectroscopy; Lac, lactate; Leu, leucine; Lys, lysine; Met, methionine; Myo, myo-inositol; NAA, N-acetyl aspartate; PCh, phosphorylcholine; PE, phosphoethanolamine; Pro, proline; Ser, serine; Suc, succinate; Tau, taurine; Thr, threonine; TOCSY, total correlation spectroscopy; Val, valine. For a detailed listing of all the labeled peak positions and assignments, see Table S2

in the ~ 4 ppm regions, suggest that both of these traces are dominated by cross-relaxation between the amide protons at 8–8.5 ppm, and the side chain ^1H s in the proteins.^{18,21,59–61} This is further validated by the MT dips arising upon irradiating the protein methyl region at ~ 1.0 ppm, which also evidence cross-relaxation with the amide region (and with water; Figure 4C). MT experiments performed by irradiating Cre's two aliphatic protons at 3.91 and 3.01 ppm (Figure 4D) also reveal features that are consistent with the L-PROSY NOESY cross-peaks, including correlations to Cre's guanidinium protons at 6.7 ppm. Cross-correlations are also evidenced for other metabolites, such as GABA. These MT profiles also highlight cross-talk with a solid-like background, which largely disappears when acquisitions are collected with longer echo times (Figure 4D); these solid-like backgrounds are invisible in the 2D L-PROSY NOESY acquisitions.

3.3 | Assignment of upfield resonances in vivo

High-field 2D NMR was also assayed for resolving murine brain metabolites in vivo. Unfortunately, the low natural abundance of ^{13}C made the acquisition of quality HSQC spectra—arguably the most informative of all the 2D experiments—incompatible with in vivo acquisition times: even

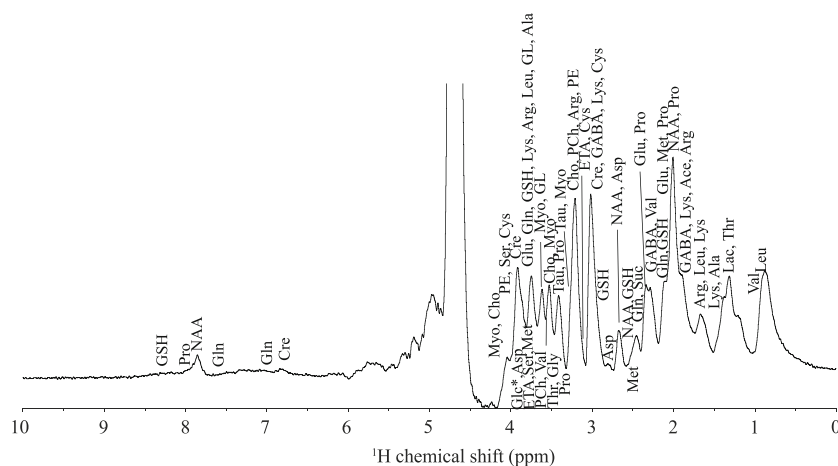


FIGURE 3 Peak assignment performed on the basis of 2D NMR acquisitions (Figures 2 and 4), indicated for a 1D 15.2-T STEAM acquisition collected *in vivo* using VAPOR-based water suppression on a 72- μ l volume, with TE/mixing/TR = 3 ms/10 ms/4 s, and 32 averages. Ace, acetate; Ala, alanine; Arg, arginine; Asp, aspartate; Cho, choline; Cre, creatine; Cys, cysteine; ETA, ethanolamine; GABA, γ -aminobutyric acid; GL, glycerol; Glc, glucose; Gln, glutamine; Glu, glutamate; Gly, glycine; GSH, glutathione; Lac, lactate; Leu, leucine; Lys, lysine; Met, methionine; Myo, myo-inositol; NAA, N-acetyl aspartate; PCh, phosphorylcholine; PE, phosphoethanolamine; Pro, proline; Ser, serine; STEAM, STimulated Echo Acquisition Mode; Suc, succinate; Tau, taurine; Thr, threonine; Val, valine; VAPOR, Variable Power radiofrequency pulses with Optimized Relaxation delays

under a low spectral resolution scenario (16 t_1 points), 12 h or longer was estimated as the minimum time required by our setup to collect these data for a full mouse brain. Instead of this experiment, we opted to perform a number of localized COSY (L-COSY)^{30,31} experiments at 15.2 T. L-COSY has been applied at lower fields on the human brain^{62–66}; the mixed-phase nature of its peaks, however, may result in streaks extending from the diagonal, and to potential cluttering among coupled and noncoupled spins. As has been demonstrated *in vivo* in large-volume (27-ml) human brain phantom studies⁶⁷ and in human bone marrow examinations,⁶⁸ this drawback is avoided by DQF counterparts.^{42,43} Localized DQF-COSY acquisitions were thus assayed at 15.2 T, both in incremented-time and in constant-time formats. The latter are associated with a sensitivity penalty, but they also provide additional line-narrowing as a result of removing J-coupling effects, and offer the possibility to remove dispersive lineshape components along the indirect domain by virtue of whole-echo acquisitions. Moreover, despite a lower sensitivity than standard COSY, we found that DQF-COSY's reliance on coherence selection gradients removed the requirement for active water suppression, while cleaning interfering background signals. To minimize artifacts both kinds of DQF-COSY experiments were implemented employing a 4:3:10 coherence selection scheme^{42,43}; these were combined with slice-refocusing gradients as shown in Figure 5A–C, to ensure minimal echo times and better experimental sensitivity. Figure 5D–F confirm the higher sensitivity of the L-COSY experiment: for instance, the signal-to-noise ratio (SNR) for the GABA4-GABA3 cross-peak was 17 ± 1 , approximately twice as those in the incremented- and constant-time DQF experiments (9.6 ± 0.9 and 9.4 ± 0.9 , respectively). Likewise, SNRs for NAA's Asp3-Asp3 cross-peaks were 86 ± 8 , 35 ± 3 , and 35 ± 3 for the three experiments in question. While suffering from an \sim two-fold penalty in SNR, the resolution of the L-DQF COSYs was markedly better than that of L-COSY, particularly in the proximity of the main diagonal. All of the experiments yielded clear identification of several cross-peaks, including those arising from GABA, Glu, Myo, NAA, Asp, Tau, phosphoethanolamine (PE), Lac, and Cho, and moieties from Lys, Glu, and GSH.

3.4 | Assessing the dynamics and environment of brain metabolites

Having resolved and assigned a number of resonances by 2D NMR, we sought to assess what these cross-peaks could report about the *in situ* dynamics of the metabolites. To do so we resorted to *ex vivo* HSQC, the experiment showing the highest resolving power, and edited these spectra according to the propensity of the correlated protons to exchange with the solvent, to undergo diffusion, or to transfer magnetization to/from proteins. HSQC experiments weighted according to WEX, diffusion weighting, and MT at selectively irradiated offsets, were thus acquired. For clarity, Figure 6 shows these results as difference 2D HSQC spectra; i.e., as the spectra arising upon applying/removing these weightings in consecutive scans, and subtracting their outputs (by receiver phase cycling for WEX, by postprocessing for the remaining experiments; see Section 2.2). Also shown are the generic pulse sequence schemes used in each of these experiments. The WEX-HSQC selected upfield resonances that have at least part of their magnetization arising via spin diffusion-assisted exchanges with the water; the diffusion-weighted (DW)-HSQC highlights the more rapidly diffusing metabolites (biased as well by a T_2 -weighting arising from the delay Δ introduced for probing diffusion by the pulsed field gradients); Δ MT-HSQC shows resonances undergoing MT with protein amides and other groups resonating at \sim 8.2 ppm (Figure S4

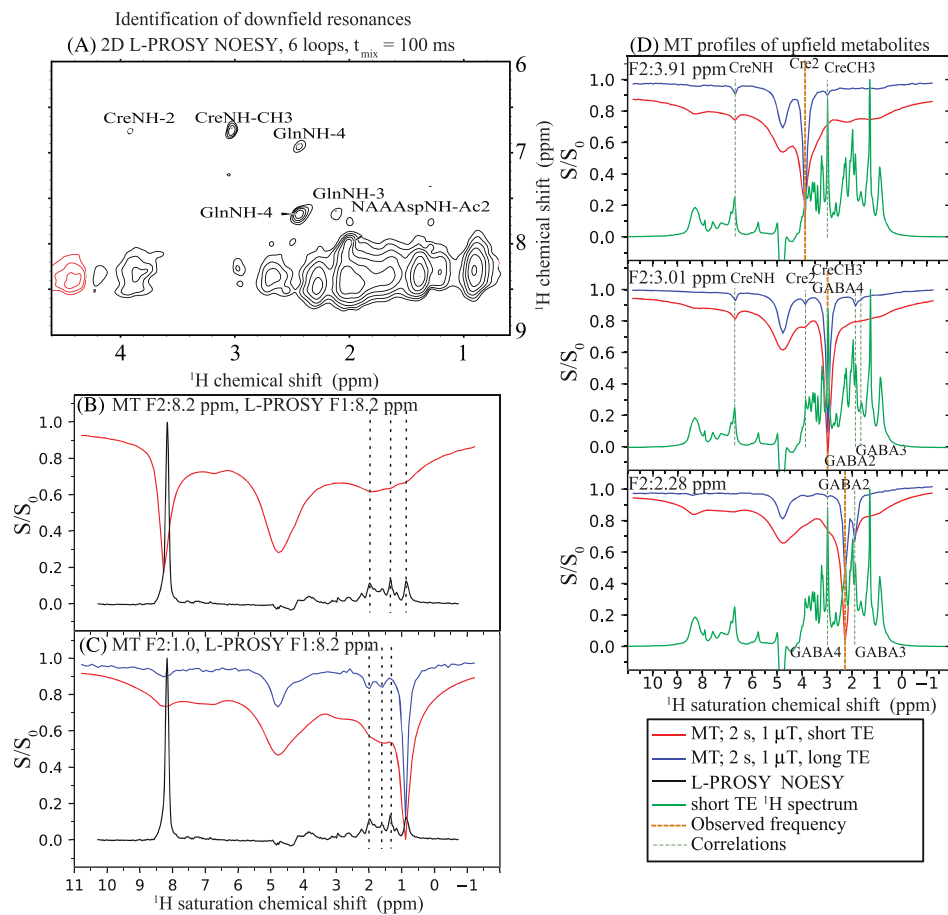


FIGURE 4 Ex vivo 14.1-T water-suppressed ^1H NMR experiments encoding cross-relaxation on a murine brain. (A) 2D L-PROSY NOESY experiment⁴⁰ performed with six loops and a 100-ms mixing time. The direct domain slice from the interaction at F1 = 8.2 ppm is depicted in (B) and (C), and compared with the MT profiles arising when the saturation frequencies were set at 8.2 ppm (b, Amides) and 1.0 ppm (c, Macromolecular aliphatic peaks). Two types of water-suppression methods were performed: WG with TE = 400 μ s, and PEW5³⁹ with TE = 40 ms. (D) MT profiles observed for the upfield resonances of Cre and GABA2, highlighting their interactions with the water and with downfield resonances. The observed F2 frequencies for each MT profile are highlighted in orange dashed lines; to facilitate the data analysis, water-suppressed spectra are shown under each trace in green. Cre, creatine; F1 and F2, indirect- and direct-domain frequencies; GABA, γ -aminobutyric acid; MT, magnetization transfer; PEW5, perfect echo sequence with W5 water suppression; TE, echo time; 2D L-PROSY NOESY, two-dimensional looped projected nuclear Overhauser effect spectroscopy; WG, WATERGATE-3919

presents a similar set, but weighted by irradiation at ~ 6.7 ppm—a chemical shift associated with Cre and with various amine/hydroxyl groups falling in this region). Figure 7 and Table S3 depict these results as ratiometric measurements, $[S_0 - S_{\text{weighted}}]/S_0$, with S_{weighted} being the magnitude of the peak in the weighted spectrum, and S_0 the magnitude of the same peak in the non-weighted HSQC.

4 | DISCUSSION

The objective of the current study was to investigate the insights that high-field 2D NMR could provide with regard to in vivo brain spectroscopy. Homonuclear 2D NMR experiments on mice appear promising, with main COSY cross-peaks emerging after ~ 18 min from a 72- μ l volume. To fully judge how our results compare with previous 2D COSY studies, it would be necessary to access the relative SNRs of the various spectra—something that is hard to assess without direct access to literature data. When considering recent 7-T human brain studies,⁶⁵ it appears that substantial sensitivity advantages arise in the animal work: in the former case, L-COSY data showing fewer cross-peaks than those in Figure 5D arose from scanning an 8.8-ml volume, ~ 100 -fold larger than those targeted here for mice. It is clear that it is not just magnetic field and cryocool differences that account for such large sensitivity differences: the ratio between the targeted volume versus the coil volume is also highly important. 2D L-COSY studies have also been reported on live mice at 9.4 and 11.7 T, targeting comparable volumes as those used in the present study.^{62,64} When comparing those spectra (e.g., fig. 2 in Ref. 64; fig. 7 in Ref. 62) with those in Figure 5D, the latter appears to be of better quality,

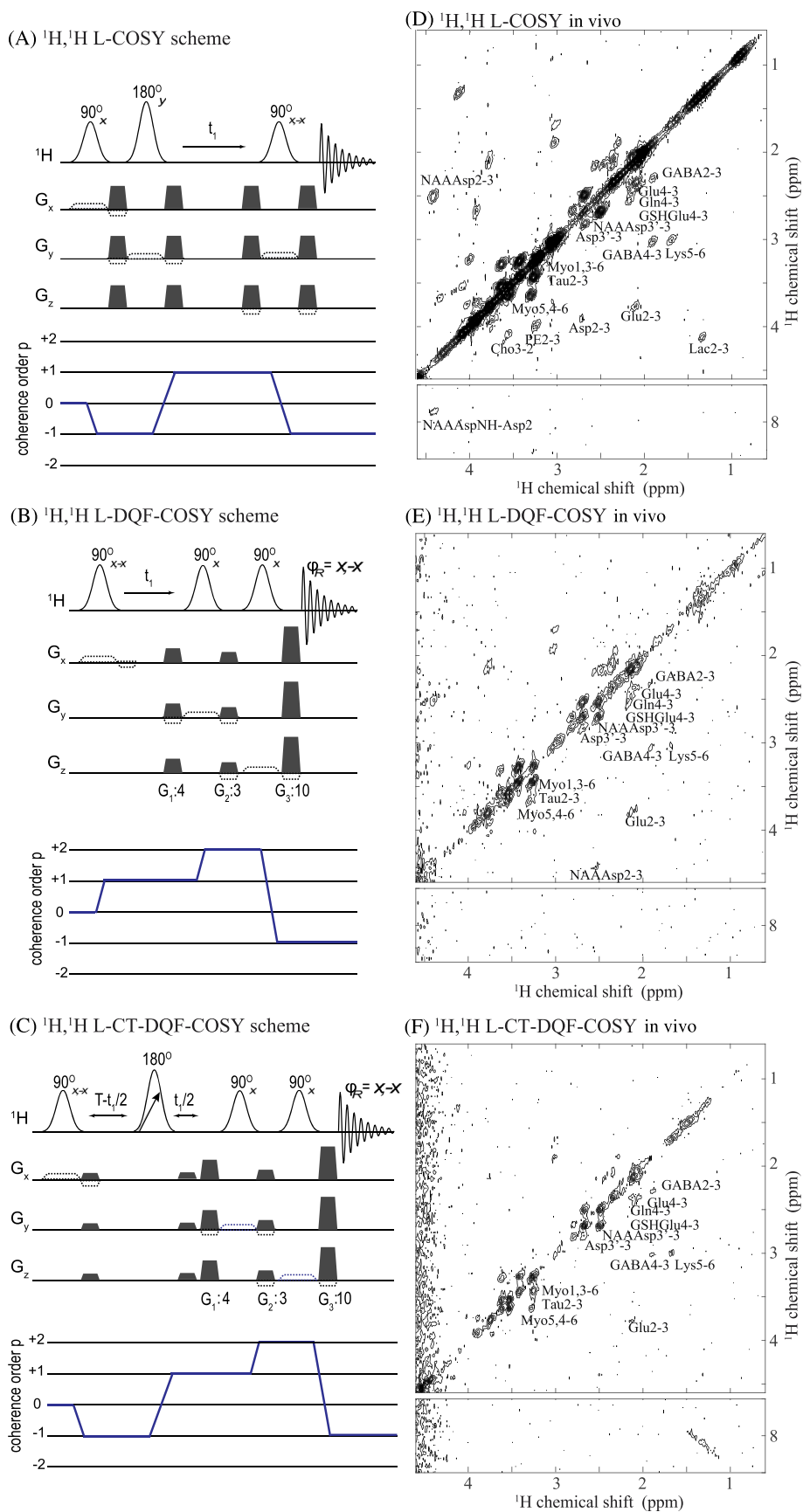


FIGURE 5 Legend on next page.

FIGURE 5 (A-C) Sequences and coherence transfer pathways (blue lines) for various L-COSY schemes; (D-F) Respective in vivo brain results obtained at 15.2 T. Spectra resulted from the co-addition of eight identical 2D datasets with two averages/ t_1 point each, recorded for a 72- μ l volume and corrected for drifts over the duration of the scan. Gaussian shapes correspond to selective pulses. Denoted in gray are the coherence selection gradients; dashed lines denote localization gradients and their refocusing lobes. When overlapping, the two kinds of gradients were activated simultaneously. All the experiments were acquired in 2 h 24 min. The L-COSY experiment was preceded by a VAPOR block prior to each scan, which was not needed in the DQF versions. The CT version employed an interval of $T = 21$ ms, and a rapid adiabatic passage π -pulse (symbolized by a diagonal arrow), incremented throughout T so as to deliver an effective echo in t_1 . See the text and Table 1 for further details. Asp, aspartate; Cho, choline; CT, constant time; DQF, double quantum-filtered; GABA, γ -aminobutyric acid; Gln, glutamine; Glu, glutamate; GSH, glutathione; Lac, lactate; L-COSY, localized correlated spectroscopy; Lys, lysine; Myo, myo-inositol; NAA, N-acetyl aspartate; Tau, taurine; VAPOR, VArable Power radiofrequency pulses with OptimizeD Relaxation delays

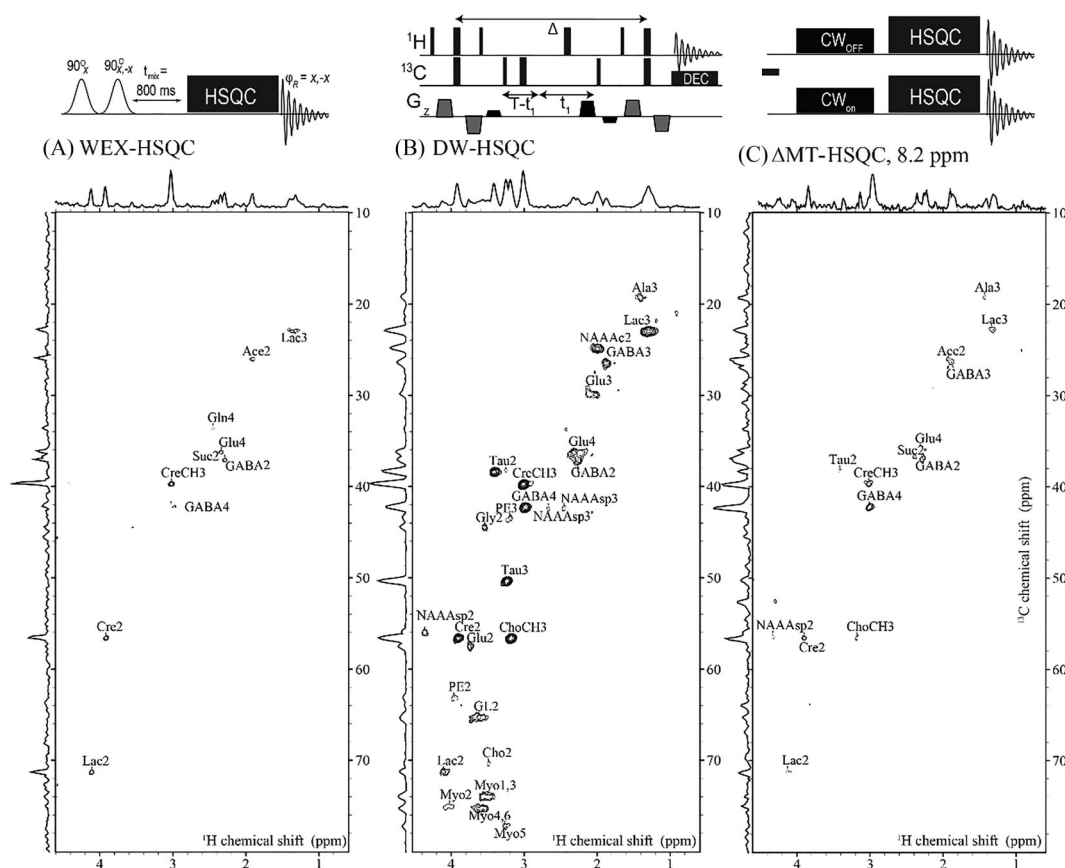


FIGURE 6 HSQC-weighted experiments arising from the pulse schemes on top, collected on excised murine brains. (A) WEX-weighted HSQC resulting from phase cycling ^1H magnetization coming from water and, after a mixing time of 800 ms, performing a suitably phase-cycled, double-resonance HSQC experiment; the full data acquisition lasted 2 h 15 min. (B) DW-HSQC arising upon subtracting a high DW-HSQC (b -value = 365 s/mm^2) from a low DW-HSQC one (b -value = 15 s/mm^2), lasting 7 h 31 min. The sequence involved a pair of constant-time HSQC acquisitions, with varying diffusion-weighting gradients (indicate in gray). Narrow and wide lines in the sequence denote 90° and 180° pulses, respectively; black gradients performed the coherence pathway selection. (C) MT-weighted HSQC resulting from subtracting a non-presaturated spectrum from one presaturated at an 8.2 ppm ^1H chemical sh, lasting 1 h 30 min. Ace, acetate; Ala, alanine; Arg, arginine; Cho, choline; Cre, creatine; DW, diffusion-weighted; GABA, γ -aminobutyric acid; GL, glycerol; Gln, glutamine; Glu, glutamate; Gly, glycine; HSQC, Heteronuclear Single Quantum Coherence Spectroscopy; Lac, lactate; MT, magnetization transfer; Myo, myo-inositol; NAA, N-acetyl aspartate; PE, phosphoethanolamine; Suc, succinate; Tau, taurine; WEX, Water EXchange filter

at least in terms of the resolution of the off-diagonal cross-peaks. Yet perhaps this is an impression deriving from the contour plot levels chosen. The number of cross-peaks resolved at 15.2 T also seems to be equal or larger than at those lower fields, yet the actual metabolites that could be identified by at least one cross-peak seems to be the same in all cases. L-DQF-COSY experiments at 15.2 T provided a clearly narrower diagonal than L-COSY, which facilitated the resolution of cross-peaks. This, however, was counteracted by a sensitivity penalty factor of ~ 2 , affecting both the real- and constant-time versions of the DQF experiment. In the end, this led to the observation of a similar number of cross-peaks for all COSY experiments.

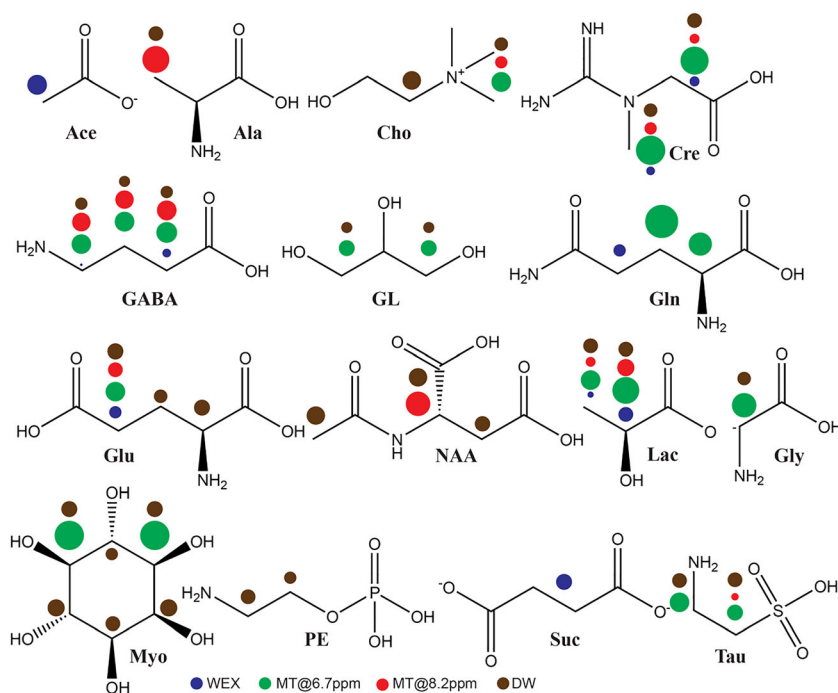


FIGURE 7 Graphical summary of the interactions found in each molecule by the edited HSQC experiments reported in Figures 6 and S4. The size of each dot is proportional to the intensity of each interaction (determined as described in the main text), with each color representing a different contrast. The results in this figure are summarized in Table S3. Ace, acetate; Ala, alanine; Arg, arginine; Cho, choline; Cre, creatine; DW, diffusion-weighted; GABA, γ -aminobutyric acid; GL, glycerol; Gln, glutamine; Glu, glutamate; Gly, glycine; HSQC, Heteronuclear Single Quantum Coherence Spectroscopy; Lac, lactate; MT, magnetization transfer; Myo, myo-inositol; NAA, N-acetyl aspartate; PE, phosphoethanolamine; Suc, succinate; Tau, taurine; WEX, Water EXchange filter

As a complement to these *in vivo* measurements, 2D NMR was also carried out on excised whole brains. Some of the *in vivo* and *ex vivo* sets of experiments (COSY, DQF-COSY) were common, and led to similar overall profiles; the main differences between the two sets pertained to sensitivity, as well as to changes in the relative intensities of certain resonances and their cross-peaks (see Table S1). One of them is lactate, a metabolite known to experience a marked postmortem increase⁴⁸; on the other hand, isoflurane-based anesthesia like that used *in vivo* can also heighten lactate concentration,⁶⁹ bringing it closer to the *ex vivo* conditions. *Ex vivo* spectra also show aspartate increasing together with a decrease in NAA; as acetate also appears to increase postmortem (its resonances are only clearly visible *ex vivo*), this probably is a side effect of NAA's breakdown.⁷⁰ A postmortem increase in GABA postmortem was also observed⁷¹; also, other metabolites displayed minor intensity variations between the *in vivo* and *ex vivo* measurements (Table S1).

The *ex vivo* measurements included ¹H-based 2D NOESY-type L-PROSY acquisitions, MT selective presaturation experiments, and WEX-based HSQC acquisitions. All these experiments yielded complementary and mutually supporting results concerning exposure to the magnetization of water's protons, which L-PROSY and MT explore through the repolarization of selectively targeted labile proton resonances, while WEX does by modulation of the full NMR spectrum according to the water magnetization. The main features worth remarking upon from these homonuclear and heteronuclear 2D water exchange and MT experiments (Figures 4, 6, 7, and S4), include: (i) the adjacency of most moieties evidencing an influence from water exchanges to carboxylate and hydroxyl groups, but not to many other kinds of labile protons that could also cause such effects; (ii) the clear correlations arising between the amide region at ~ 8.2 ppm, and both α and sidechain protein or peptide protons in the upfield region; (iii) the additional interactions that metabolites such as GABA, NAA, and Cre show within the molecules in the metabolite-detected MT profiles, the L-PROSY NOESY spectra, and the Δ MT-HSQC experiments; (iv) the mostly charged nature of most small metabolites that show magnetization transfers to/from the 6.7-ppm region, probably highlighting (in addition to NAA's protons) other amines and hydroxyl groups. Some of these features—foremost the MT effects—have been noted in the literature^{19,72}; however, the 2D NOESY and HSQC acquisitions provide a substantial spectral resolution improvement on the data (e.g., Figure 4B,C), which sheds light on the specificity of the exchange and MT effects observed.

As can be seen by comparing the conventional and the DW *ex vivo* HSQC spectra in Figures 2 and 6, the signatures of many metabolites disappear upon applying diffusivity-weighting gradients; this, despite the fact that diffusivity is lowered under postmortem conditions.⁷³ Further inspection of Figures 6 and 7 evidences a correlation between metabolites showing slower diffusivities (as highlighted by the DW-HSQC experiments), and those showing more substantial MT throughout their molecules. This could reflect the facilitation of polarization transfer effects

for slower-diffusing metabolites as a result of them residing in more restricted compartments, or from their interaction with proteins that facilitate spin diffusion but slow down their overall correlation times. This would also explain the solid-like MTs in Figure 4D for both GABA and Cre, as well as the Δ MT-HSQC peaks that these metabolites show in Figure 6C. This conjecture could benefit from further spatially localized studies in specific areas of the brain, such as white matter-rich regions.

5 | CONCLUSIONS

The current study discusses some of the promising avenues opening in brain spectroscopy in the advent of 2D high-field NMR. Clearly, the resolving ability of in vivo experiments is lower than that of ex vivo observations—particularly when considering heteronuclear correlations, which enable the identification of an unprecedented number of metabolites from an intact brain. Ex vivo experiments also revealed correlations involving the labile protons of Gln and proline, as well as previously known cross-peaks (e.g., those from NAA and GSH). Cre guanidinium protons could also be unambiguously identified in MT and L-PROSY experiments (Figure 4), as well as by 2D COSY (Figure 2B). These ex vivo observations can potentially be added to basis sets seeking to interpret localized in vivo 1D NMR experiments of the downfield region.

2D NMR efforts generally focus on resolving and quantifying the abundance of individual metabolites. By facilitating the resolution of metabolic signatures, these experiments also open a number of alternative investigative avenues. This study, for instance, also focused on exploring how these measurements can serve to probe molecular environments, including cross-relaxation, exposure to water and biomacromolecules, and diffusivity. This in turn can be useful to account for results obtained in other kinds of low resolution but amply used 1D NMR experiments, such as water-detected CEST, MT, and DW 1 H MRS. Incorporating studies of specific regions of the brain into these procedures—including the addition of spatially encoded dimensions—could provide an even clearer picture of the specific dynamics of different metabolites in white matter- or gray matter-rich areas. It also remains to be seen if, with the use of partial isotopic enrichment, heteronuclear correlations can also be added to these investigations.

ACKNOWLEDGMENTS

The authors thank Dr. Mihajlo Novakovic for help with the NMR experiments, Dr. Assaf Tal for valuable discussions, Keren Sasson and Anna Tatarin for help in animal handling, Dr. Yasvir Tesiram for sequence programming help, and Odelia Chitrit and Dr. Talia Harris for help with setting up the in vivo experiments. This work was supported by the Clore Institute for Magnetic Resonance (Weizmann Institute), the Israel Science Foundation (grants 3594/21 and 1874/22), and the EU Horizon 2020 programme (Marie Skłodowska-Curie Grant 642773 and FET-OPEN PATHOS grant 828946).

ORCID

Lucio Frydman  <https://orcid.org/0000-0001-8208-3521>

REFERENCES

1. van Essen D, Smith SM, Barch DM, et al. The WU-Minn Human Connectome Project: An overview. *NeuroImage*. 2013;80:62-79. doi:10.1016/j.neuroimage.2013.05.041
2. Atlas SW. *Magnetic Resonance Imaging of the Brain and Spine*. 5th ed. Wolters Kluwer; 2017.
3. van der Graaf M. In vivo magnetic resonance spectroscopy: basic methodology and clinical applications. *Eur Biophys J*. 2010;39(4):527-540. doi:10.1007/s00249-009-0517-y
4. Duarte JMN, Lei H, Mlynárik V, Gruetter R. The neurochemical profile quantified by in vivo 1 H NMR spectroscopy. *NeuroImage*. 2012;61(2):342-362. doi:10.1016/j.neuroimage.2011.12.038
5. Öz G, Alger JR, Barker PB, et al. Clinical proton MR spectroscopy in central nervous system disorders. *Radiology*. 2014;270(3):658-679. doi:10.1148/radiol.13130531
6. Hwang JH, Choi CS. Use of in vivo magnetic resonance spectroscopy for studying metabolic diseases. *Exp Mol Med*. 2015;47:1-8.
7. de Graaf RA. *Vivo NMR Spectroscopy: Principles and Techniques*. 3rd ed. John Wiley & Sons; 2019.
8. Ronen I, Valette J. Diffusion-weighted magnetic resonance spectroscopy. *E Mag Res*. 2015;4:733-750. doi:10.1002/9780470034590.emrstm1471
9. Palombo M, Shemesh N, Ronen I, Valette J. Insights into brain microstructure from in vivo DW-MRS. *NeuroImage*. 2018;182:97-116. doi:10.1016/j.neuroimage.2017.11.028
10. Vincent M, Palombo M, Valette J. Revisiting double diffusion encoding MRS in the mouse brain at 11.7T: Which microstructural features are we sensitive to? *NeuroImage*. 2020;207:116399 doi:10.1016/j.neuroimage.2019.116399
11. Morrison C, Henkelman RM. A model for magnetization transfer in tissues. *Magn Reson Med*. 1995;33(4):475-482. doi:10.1002/mrm.1910330404
12. Henkelman RM, Stanisz GJ, Graham SJ. Magnetization transfer in MRI: A review. *NMR Biomed*. 2001;14(2):57-64. doi:10.1002/nbm.683
13. van Gelderen P, Jiang X, Duyn JH. Effects of magnetization transfer on T1 contrast in human brain white matter. *NeuroImage*. 2016;128:85-95. doi:10.1016/j.neuroimage.2015.12.032
14. Ward KM, Aletras AH, Balaban RS. A new class of contrast agents for MRI based on proton chemical exchange dependent saturation transfer (CEST). *J Magn Reson*. 2000;143(1):79-87. doi:10.1006/jmre.1999.1956

15. Zhou J, van Zijl PCM. Chemical exchange saturation transfer imaging and spectroscopy. *Prog Nucl Magn Reson Spectrosc.* 2006;48(2–3):109–136. doi: [10.1016/j.pnmrs.2006.01.001](https://doi.org/10.1016/j.pnmrs.2006.01.001)
16. Van Zijl PCM, Yadav NN. Chemical exchange saturation transfer (CEST): What is in a name and what isn't? *Magn Reson Med.* 2011;65(4):927–948. doi: [10.1002/mrm.22761](https://doi.org/10.1002/mrm.22761)
17. van Zijl PCM, Lam WW, Xu J, Knutsson L, Stanisz GJ. Magnetization transfer contrast and chemical exchange saturation transfer MRI. Features and analysis of the field-dependent saturation spectrum. *NeuroImage.* 2018;168:222–241. doi: [10.1016/j.neuroimage.2017.04.045](https://doi.org/10.1016/j.neuroimage.2017.04.045)
18. Zhou J, Lal B, Wilson DA, Larterra J, Van Zijl PCM. Amide proton transfer (APT) contrast for imaging of brain tumors. *Magn Reson Med.* 2003;50(6):1120–1126. doi: [10.1002/mrm.10651](https://doi.org/10.1002/mrm.10651)
19. Lee JS, Xia D, Jerschow A, Regatte RR. In vitro study of endogenous CEST agents at 3T and 7T. *Contrast Media Mol Imaging.* 2016;11(1):4–14. doi: [10.1002/cmim.1652](https://doi.org/10.1002/cmim.1652)
20. Zu Z, Louie EA, Lin EC, et al. Chemical exchange rotation transfer imaging of intermediate-exchanging amines at 2 ppm. *NMR Biomed.* 2017;30(10):e3756. doi: [10.1002/nbm.3756](https://doi.org/10.1002/nbm.3756)
21. Chen L, Wei Z, Chan KWY, et al. Protein aggregation linked to Alzheimer's disease revealed by saturation transfer MRI. *NeuroImage.* 2019;188:380–390. doi: [10.1016/j.neuroimage.2018.12.018](https://doi.org/10.1016/j.neuroimage.2018.12.018)
22. Budinger TF, Bird MD, Frydman L, et al. Toward 20 T magnetic resonance for human brain studies: opportunities for discovery and neuroscience rationale. *Magn Reson Mater Physics, Biol Med.* 2016;29(3):617–639. doi: [10.1007/s10334-016-0561-4](https://doi.org/10.1007/s10334-016-0561-4)
23. Ladd ME, Bachert P, Meyerspeer M, et al. Pros and cons of ultra-high-field MRI/MRS for human application. *Prog Nucl Magn Reson Spectrosc.* 2018;109:1–50. doi: [10.1016/j.pnmrs.2018.06.001](https://doi.org/10.1016/j.pnmrs.2018.06.001)
24. Pfeuffer J, Tkáč I, Provencher SW, Gruetter R. Toward an in vivo neurochemical profile: quantification of 18 metabolites in short-echo-time 1H NMR spectra of the rat brain. *J Magn Reson.* 1999;141(1):104–120. doi: [10.1006/jmre.1999.1895](https://doi.org/10.1006/jmre.1999.1895)
25. Jansen JFA, Backes WH, Nicolay K, Kooi ME. 1H MR spectroscopy of the brain: Absolute quantification of metabolites. *Radiology.* 2006;240(2):318–332. doi: [10.1148/radiol.2402050314](https://doi.org/10.1148/radiol.2402050314)
26. Elliott SJ, Bengs C, Kouril K, et al. NMR lineshapes and scalar relaxation of the water-endofullerene H217O@C60. *Chem Phys Chem.* 2018;19(3):251–255. doi: [10.1002/cphc.201701330](https://doi.org/10.1002/cphc.201701330)
27. Bogner W, Hangel G, Esmaili M, Andronesi OC. 1D-spectral editing and 2D multispectral in vivo 1H-MRS and 1H-MRSI - Methods and applications. *Anal Biochem.* 2017;529:48–64. doi: [10.1016/j.ab.2016.12.020](https://doi.org/10.1016/j.ab.2016.12.020)
28. Cavanagh J, Fairbrother WJ, Palmer AG III, Rance M, Skelton NJ. *Protein NMR Spectroscopy.* 2nd ed. Elsevier; 2007.
29. Keeler J. *Understanding NMR Spectroscopy.* Wiley; 2002.
30. Thomas MA, Yue K, Binesh N, et al. Localized two-dimensional shift correlated MR spectroscopy of human brain. *Magn Reson Med.* 2001;46(1):58–67. doi: [10.1002/mrm.1160](https://doi.org/10.1002/mrm.1160)
31. Thomas MA, Hattori N, Umeda M, Sawada T, Naruse S. Evaluation of two-dimensional L-COSY and JPRESS using a 3 T MRI scanner: From phantoms to human brain in vivo. *NMR Biomed.* 2003;16(5):245–251. doi: [10.1002/nbm.825](https://doi.org/10.1002/nbm.825)
32. Iglesias JE, Crampsie S, Strand C, Tachrount M, Thomas DL, Holton JL. Effect of fluorinert on the histological properties of formalin-fixed human brain tissue. *J Neuropathol Exp Neurol.* 2018;77(12):1085–1090. doi: [10.1093/jnen/nly098](https://doi.org/10.1093/jnen/nly098)
33. Boonstra JT, Michielse S, Roebroek A, Temel Y, Jahanshahi A. Dedicated magnetite for postmortem human brain ultra-high field magnetic resonance imaging. *NeuroImage.* 2021;235:118010. doi: [10.1016/j.neuroimage.2021.118010](https://doi.org/10.1016/j.neuroimage.2021.118010)
34. Wishart DS, Bigam CG, Yao J, et al. 1H, 13C and 15N chemical shift referencing in biomolecular NMR. *J Biomol NMR.* 1995;6(2):135–140. doi: [10.1007/BF00211777](https://doi.org/10.1007/BF00211777)
35. Wishart DS, Tzur D, Knox C, et al. HMDB: The human metabolome database. *Nucleic Acids Res.* 2007;35:521–526. doi: [10.1093/nar/gkl923](https://doi.org/10.1093/nar/gkl923)
36. Wishart DS, Feunang YD, Marcu A, et al. HMDB 4.0: The human metabolome database for 2018. *Nucleic Acids Res.* 2018;46(D1):D608–D617. doi: [10.1093/nar/gkx1089](https://doi.org/10.1093/nar/gkx1089)
37. Piotto M, Saudek V, Sklenář V. Gradient-tailored excitation for single-quantum NMR spectroscopy of aqueous solutions. *J Biomol NMR.* 1992;2(6):661–665. doi: [10.1007/BF02192855](https://doi.org/10.1007/BF02192855)
38. Sklenář V, Piotto M, Leppik R, Saudek V. Gradient-tailored water suppression for 1H-15N HSQC experiments optimized to retain full sensitivity. *J Magn Reson - Ser A.* 1993;102(2):241–245. doi: [10.1006/jmra.1993.1098](https://doi.org/10.1006/jmra.1993.1098)
39. Adams RW, Holroyd CM, Aguilar JA, Nilsson M, Morris GA. "Perfecting" WATERGATE: Clean proton NMR spectra from aqueous solution. *Chem Commun.* 2013;49(4):358–360. doi: [10.1039/C2CC37579F](https://doi.org/10.1039/C2CC37579F)
40. Novakovic M, Cousin SF, Jaroszewicz MJ, Rosenzweig R, Frydman L. Looped-PROjected Spectroscopy (L-PROSY): A simple approach to enhance backbone/sidechain cross-peaks in 1H NMR. *J Magn Reson.* 2018;294:169–180. doi: [10.1016/j.jmr.2018.07.010](https://doi.org/10.1016/j.jmr.2018.07.010)
41. Emsley L, Bodenhausen G. Gaussian pulse cascades: New analytical functions for rectangular selective inversion and in-phase excitation in NMR. *Chem Phys Lett.* 1990;165(6):469–476. doi: [10.1016/0009-2614\(90\)87025-M](https://doi.org/10.1016/0009-2614(90)87025-M)
42. Shaw AA, Salaun C, Dauphin JF, Ancian B. Artifact-free PFG-enhanced double-quantum-filtered COSY experiments. *J Magn Reson - Ser A.* 1996;120(1):110–115. doi: [10.1006/jmra.1996.0105](https://doi.org/10.1006/jmra.1996.0105)
43. Ancian B, Bourgeois I, Dauphin JF, Shaw AA. Artifact-free pure absorption PFG-enhanced DQF-COSY spectra including a gradient pulse in the evolution period. *J Magn Reson.* 1997;125(2):348–354. doi: [10.1006/jmre.1997.1112](https://doi.org/10.1006/jmre.1997.1112)
44. Rucker S, Shaka AJ. Broadband homonuclear cross polarization in 2D N.M.R. using DIPSI-2. *Mol Phys.* 1989;68(2):509–517. doi: [10.1080/00268978900102331](https://doi.org/10.1080/00268978900102331)
45. Mori S, van Zijl PCM, Johnson MON, Berg JM. Water exchange filter (WEX filter) for nuclear magnetic resonance studies of macromolecules. *J Am Chem Soc.* 1994;116(26):11982–11984. doi: [10.1021/ja00105a044](https://doi.org/10.1021/ja00105a044)
46. McLachlan AS, Richards JJ, Bilia AR, Morris GA. Constant time gradient HSQC-iDOSY: Practical aspects. *Magn Reson Chem.* 2009;47(12):1081–1085. doi: [10.1002/mrc.2518](https://doi.org/10.1002/mrc.2518)
47. Lee W, Tonelli M, Markley JL. NMRFAM-SPARKY: Enhanced software for biomolecular NMR spectroscopy. *Bioinformatics.* 2015;31(8):1325–1327. doi: [10.1093/bioinformatics/btu830](https://doi.org/10.1093/bioinformatics/btu830)
48. Musshoff F, Klotzbach H, Block W, Traeber F, Schild H, Madea B. Comparison of post-mortem metabolic changes in sheep brain tissue in isolated heads and whole animals using 1H-MR spectroscopy-preliminary results. *Int J Leg Med.* 2011;125(5):741–744. doi: [10.1007/s00414-010-0463-3](https://doi.org/10.1007/s00414-010-0463-3)

49. Kruk J, Doskocz M, Jodłowska E, et al. NMR techniques in metabolomic studies: a quick overview on examples of utilization. *Appl Magn Reson*. 2017; 48(1):1-21. doi:[10.1007/s00723-016-0846-9](https://doi.org/10.1007/s00723-016-0846-9)
50. Maroli AS, Powers R. Closing the gap between in vivo and in vitro omics: using QA/QC to strengthen ex vivo NMR metabolomics. *NMR Biomed*. 2021; 1-14:e4594.
51. Lu W, Su X, Klein MS, Lewis IA, Fiehn O, Rabinowitz JD. Metabolite measurement: Pitfalls to avoid and practices to follow. *Annu Rev Biochem*. 2017; 86(1):277-304. doi:[10.1146/annurev-biochem-061516-044952](https://doi.org/10.1146/annurev-biochem-061516-044952)
52. Barekatin Y, Yan VC, Arthur K, et al. Robust detection of oncometabolic aberrations by ¹H-¹³C heteronuclear single quantum correlation in intact biological specimens. *Commun Biol*. 2020;3(1):328. doi:[10.1038/s42003-020-1055-5](https://doi.org/10.1038/s42003-020-1055-5)
53. Park GHJ, Yang S, Baek H. 900MHz ¹H-/¹³C-NMR analysis of 2-hydroxyglutarate and other brain metabolites in human brain tumor tissue extracts. *PLoS ONE*. 2018;13(9):e0203379. doi:[10.1371/journal.pone.0203379](https://doi.org/10.1371/journal.pone.0203379)
54. Grande S, Luciani AM, Rosi A, Guidoni L, Viti V. Identification of amide protons of glutathione in MR spectra of tumour cells. *NMR Biomed*. 2008; 21(10):1057-1065. doi:[10.1002/nbm.1280](https://doi.org/10.1002/nbm.1280)
55. Wuthrich K. *NMR of Proteins and Nucleic Acids*. Vol. 17. 1st ed. Wiley-Interscience; 1986:11-13. doi:[10.1051/epn/19861701011](https://doi.org/10.1051/epn/19861701011).
56. Kruskamp MJ, De Graaf RA, Van Vliet G, Nicolay K. Magnetic coupling of creatine/phosphocreatine protons in rat skeletal muscle, as studied by ¹H-magnetization transfer MRS. *Magn Reson Med*. 1999;42(4):665-672. doi:[10.1002/\(SICI\)1522-2594\(199910\)42:4%3C665::AID-MRM7%3E3.0.CO;2-9](https://doi.org/10.1002/(SICI)1522-2594(199910)42:4%3C665::AID-MRM7%3E3.0.CO;2-9)
57. De Graaf RA, Van Kranenburg A, Nicolay K. Off-resonance metabolite magnetization transfer measurements on rat brain in situ. *Magn Reson Med*. 1999;41(6):1136-1144. doi:[10.1002/\(SICI\)1522-2594\(199906\)41:6%3C1136::AID-MRM9%3E3.0.CO;2-G](https://doi.org/10.1002/(SICI)1522-2594(199906)41:6%3C1136::AID-MRM9%3E3.0.CO;2-G)
58. Leibfritz D, Dreher W. Magnetization transfer MRS. *NMR Biomed*. 2001;14(2):65-76. doi:[10.1002/nbm.681](https://doi.org/10.1002/nbm.681)
59. Zhou J, Payen J-F, Wilson D, Traystman R, Van Zijl P. Using the amide proton signals of intracellular proteins and peptides to detect pH effects in MRI. *Nat Med*. 2003;9(8):1085-1090. doi:[10.1038/nm907](https://doi.org/10.1038/nm907)
60. Tietze A, Blicher J, Mikkelsen IK, et al. Assessment of ischemic penumbra in patients with hyperacute stroke using amide proton transfer (APT) chemical exchange saturation transfer (CEST) MRI. *NMR Biomed*. 2014;27(2):163-174. doi:[10.1002/nbm.3048](https://doi.org/10.1002/nbm.3048)
61. Togao O, Yoshiura T, Keupp J, et al. Amide proton transfer imaging of adult diffuse gliomas: Correlation with histopathological grades. *Neuro Oncol*. 2014;16(3):441-448. doi:[10.1093/neuonc/not158](https://doi.org/10.1093/neuonc/not158)
62. Braakman N, Oerther T, De Groot HJM, Alia A. High resolution localized two-dimensional MR spectroscopy in mouse brain in vivo. *Magn Reson Med*. 2008;60(2):449-456. doi:[10.1002/mrm.21662](https://doi.org/10.1002/mrm.21662)
63. Verma G, Hariharan H, Nagarajan R, et al. Implementation of two-dimensional L-COSY at 7 Tesla: An investigation of reproducibility in human brain. *J Magn Reson Imaging*. 2014;40(6):1319-1327. doi:[10.1002/jmri.24510](https://doi.org/10.1002/jmri.24510)
64. Martel D, Tse Ve Koon K, Le Fur Y, Ratiney H. Localized 2D COSY sequences: Method and experimental evaluation for a whole metabolite quantification approach. *J Magn Reson*. 2015;260:98-108. doi:[10.1016/j.jmr.2015.09.002](https://doi.org/10.1016/j.jmr.2015.09.002)
65. Verma G, Mohan S, Nasrallah MLP, et al. Non-invasive detection of 2-hydroxyglutarate in IDH-mutated gliomas using two-dimensional localized correlation spectroscopy (2D L-COSY) at 7 Tesla. *J Transl Med*. 2016;14(1):1-8. doi:[10.1186/s12967-015-0757-9](https://doi.org/10.1186/s12967-015-0757-9)
66. Tosh N, Quadrelli S, Galloway G, Mountford C. Two new fucose- α (1-2)-glycans assigned in the healthy human brain taking the number to seven. *Sci Rep*. 2019;9(1):1-8. doi:[10.1038/s41598-019-54933-1](https://doi.org/10.1038/s41598-019-54933-1)
67. Ryner LN, Sorenson JA, Thomas MA. 3D localized 2D NMR spectroscopy on an MRI scanner. *J Magn Reson Ser B*. 1995;107(2):126-137. doi:[10.1006/jmrb.1995.1068](https://doi.org/10.1006/jmrb.1995.1068)
68. Prescott AP, Dzik-Jurasz ASK, Leach MO, Sirohi B, Powles R, Collins DJ. Localized COSY and DQF-COSY ¹H-MRS sequences for investigating human tibial bone marrow in vivo and initial application to patients with acute leukemia. *J Magn Reson Imaging*. 2005;22(4):541-548. doi:[10.1002/jmri.20413](https://doi.org/10.1002/jmri.20413)
69. Makaryus R, Lee H, Yu M, et al. The metabolomic profile during isoflurane anesthesia differs from propofol anesthesia in the live rodent brain. *J Cereb Blood Flow Metab*. 2011;31(6):1432-1442. doi:[10.1038/jcbfm.2011.1](https://doi.org/10.1038/jcbfm.2011.1)
70. Cheng LL, Ma MJ, Becerra L, et al. Quantitative neuropathology by high resolution magic angle spinning proton magnetic resonance spectroscopy. *Proc Natl Acad Sci U S A*. 1997;94(12):6408-6413. doi:[10.1073/pnas.94.12.6408](https://doi.org/10.1073/pnas.94.12.6408)
71. van der Heyden JAM, Korf J. Regional levels of GABA in the brain: rapid semiautomated assay and prevention of postmortem increase by 3-mercapto-propionic acid. *J Neurochem*. 1978;31(1):197-203. doi:[10.1111/j.1471-4159.1978.tb12448.x](https://doi.org/10.1111/j.1471-4159.1978.tb12448.x)
72. Cai K, Haris M, Singh A, et al. Magnetic resonance imaging of glutamate. *Nat Med*. 2012;18(2):302-306. doi:[10.1038/nm.2615](https://doi.org/10.1038/nm.2615)
73. Widjaja E, Wei X, Vidarsson L, Moineddin R, Macgowan CK, Nilsson D. Alteration of diffusion tensor parameters in postmortem brain. *Magn Reson Imaging*. 2009;27(6):865-870. doi:[10.1016/j.mri.2008.11.009](https://doi.org/10.1016/j.mri.2008.11.009)

SUPPORTING INFORMATION

Additional supporting information can be found online in the Supporting Information section at the end of this article.

How to cite this article: Martinho RP, Jain MG, Frydman L. High-field ex vivo and in vivo two-dimensional nuclear magnetic resonance spectroscopy in murine brain: Resolving and exploring the molecular environment. *NMR in Biomedicine*. 2023;36(2):e4833. doi:[10.1002/nbm.4833](https://doi.org/10.1002/nbm.4833)